ITERATIVE ELECTRODE CONTACT DESIGN
FOR EFFICIENT NEURAL STIMULATION

Authors:
Naina Iyengar and Andrew DeMaria

Faculty Sponsor:
Xuefeng Wei,
Department of Biomedical Engineering

ABSTRACT

Deep brain stimulation (DBS) is a clinically proven therapy of electrically stimulating specific brain structures such as the subthalamic nucleus (STN), via surgically implanted electrodes, to treat neurological disorders such as Parkinson's disease. Our study involved designing novel electrode contact geometries, based on mathematically defined sequences, which would generate a larger simulated volume of tissue activated (VTA), and would therefore be more power-efficient, than that of the standard cylindrical electrode geometry. Spatial voltage distribution in a grey matter tissue medium generated by these electrodes, using finite element models (FEM), were interpolated and applied to a population of neurons represented by multi-compartment cable models with mammalian membrane dynamics. Thresholds of activation for these model neurons were simulated to generate three-dimensional solids representing the VTAs. Using this method, our novel electrodes with first three shape iterations proved to activate a 23.9%, 28.3%, and 29.4% larger tissue volume and were thus more efficient than a conventional electrode.

INTRODUCTION

Deep brain stimulation (DBS) is an FDA-approved stereotactic therapy used to treat medically refractory neuromotor disorders such as Parkinson's disease (PD), essential tremor (ET), and dysotonia, and has been suggested for cognitive-behavioral dysfunctions such as obsessive-compulsive disorder and clinical depression (Benabid *et al.*, 2009; Chopra *et al.*, 2013; Hu and Stead, 2014; Fontaine *et al.*, 2004; Holtzheimer III and Mayberg, 2010). DBS has been clinically effective in reducing symptoms of these conditions; one study observed a 96% decrease in the severity of levodopa-induced dyskinesias in PD DBS patients (Russman *et al.*, 2004). Neurosurgical implantation commonly involves bilateral subthalamic nucleus (STN) placement of biocompatible electrode leads connected by an extension wire to a subcutaneous primary cell battery-powered implantable pulse generator (IPG) within the subclavicular tissue (Dorvad *et al.*, 2009; Kawakami *et al.*, 2005). IPGs possess a finite battery lifetime, which can be as low as 2 years in pallidal high-charge stimulation in dysotonia patients, and so must be periodically replaced (Blahak *et al.*, 2001). However, each surgical placement and replacement is a costly feat carrying many risks such as hardware complications and infection, which may facilitate subsequent removal and replacement (Groiss *et al.*, 2009). For instance, a study involving 270 DBS participants found that full hardware removal was necessitated in 48.5% of patients who had developed post-operative infection, with an increased risk when *Stapholococcus aureus* was the infectious pathogen (Bhatia *et al.*, 2010).

It has been shown that the activating function of a neuron, which is proportional to the second spatial derivative of its extracellular potential and thereby the spatial derivative of surface current density, can predict its neural excitability (Rattay 1989). The spatial derivative of surface current density, in turn, can be increased by the utilization of high-perimeter electrode geometries (Wei and Grill, 2009), as current density increases towards the perimeters (edges) of electrode surface. The mathematical basis of this is described by the equation below (Wei and Grill, 2009):

$$f(x) = \Delta^2 V_e / \Delta x^2 = \Delta(\Delta V_e/\Delta x) = \Delta(J_x/\text{-}\sigma)/\Delta x = \Delta J_x/(\text{-}\sigma\Delta x),$$

where V_e is extracellular potential, $\Delta J_x /\Delta x$ is spatial derivative of current density in x direction, and σ is conductivity (S/m).

The final activation of vicinal neurons has been quantitatively measured through a calculation of the volume of tissue activated (VTA) for a given design (Butson and McIntyre, 2006). A previous study showed a 22% simulated increase in efficiency when fractal designs, namely Sierpinski carpet fractals, were applied to planar electrodes (Golestanirad *et al.*, 2013). However, VTAs for cylindrical fractal electrodes have not yet been explored. Therefore, our study aimed to increase stimulation power efficiency of DBS leads by fractal-like computational remodeling of conventional cylindrical electrodes by increasing contact perimeter, thereby increasing battery lifetime and by extension, decreasing the frequency of surgical IPG replacements. Since this study only involves reshaping of contact geometries using existing materials (i.e. platinum-iridium alloy, etc.), the extensive biocompatibility testing procedures necessitated by the utilization of new materials can be eluded.

MATERIALS AND METHODS

Iterative Contact Design: Standard electrode dimensions based on the Medtronic, Inc. Lead No. 3389 were implemented in this study using SolidWorks 2013 x64 Edition (SolidWorks Corp., Waltham, MA) consisting of a diameter of 1.27 mm, a proximal tip length of 9.25 mm, and a rounded distal tip end of 1.5 mm (Coffrey, 2009); one electrode contact was used. Electrode contact geometries were chosen such that they had the same final surface area, despite higher perimeters, as a conventional electrode (Chart 1).

Chart 1. Contact Geometry Properties

Prototype ID	Segment length (mm)	Area (mm^2)	Area ratio	Perimeter (mm)	Perimeter ratio
1	1.50	5.985	100%	7.98	100.00%
2	2.50	5.985	100%	31.98	400.75%
3	2.90	5.985	100%	46.38	581.20%
4	3.02	5.985	100%	59.34	743.61%

Our electrode contact designs were based on a novel criss-cross shape consisting of a base band, and at least one periodic protrusion extending in both vertical directions (i.e. two rays starting at the contact center point and running along the main axis of electrode length towards the two ends), which were defined by specific parameters (Figure 1a). These parameters describe additions of fractal-like iterative compressions of protrusions to 30% of its previous height, and subtraction of an equal area from, each horizontal edge (Figure 1b). In essence, areas of height $2P_n/3$ were added to the middle 1/3 of, while areas of height $P_n/3$ were simultaneously subtracted from the two outer 1/3's of, the specified edges; this ensured a constant surface area and a net protrusion of $2P_n/3+P_n/3=P_n$ (Figure 1c).

1(a).

1. Protrusion height, P_n: 0.3^n where $n \geq 0$

2. Base height, B_n: $B_{n-1} - \dfrac{2m \cdot P_n}{3}$ where $B_{-1}=0.5$; $m = \begin{cases} 0, n=0 \\ 1, n>0 \end{cases}$

1(b).

Chart 1. Iterative Height Measurements (mm) Using Defined Parameters.

n	B_n	P_0	P_1	P_2	P_3
0	0.5	1	X	X	X
1	0.3	1	0.3	X	X
2	0.24	1	0.3	0.09	X

Note: the maximum height$_n$ (i.e. from the center-most protrusion P_n on P_0 in one vertical direction to the center-most protrusion P_n on P_0 in the other vertical direction) is $B_n+2[P_0+P_1+...P_n]$.
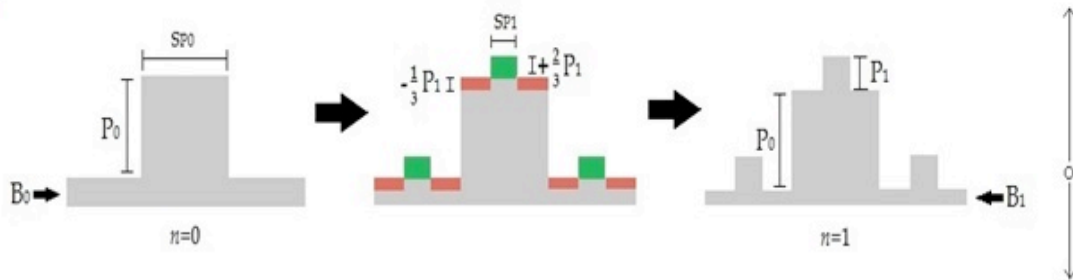
1 (c).

Figure 1. Construction of Iterative Electrodes. 1(a): Equations on which iterative contact construction were based. 1(b) Sequential expansion with each n. 1(c) Simultaneous addition-subtraction during the creation of electrode$_1$ from electrode$_0$. Note that for demonstrative purposes, contacts are modelled as planar instead of curved, are not to scale, and height deduction in only one vertical direction (i.e. about half the contact) is shown.
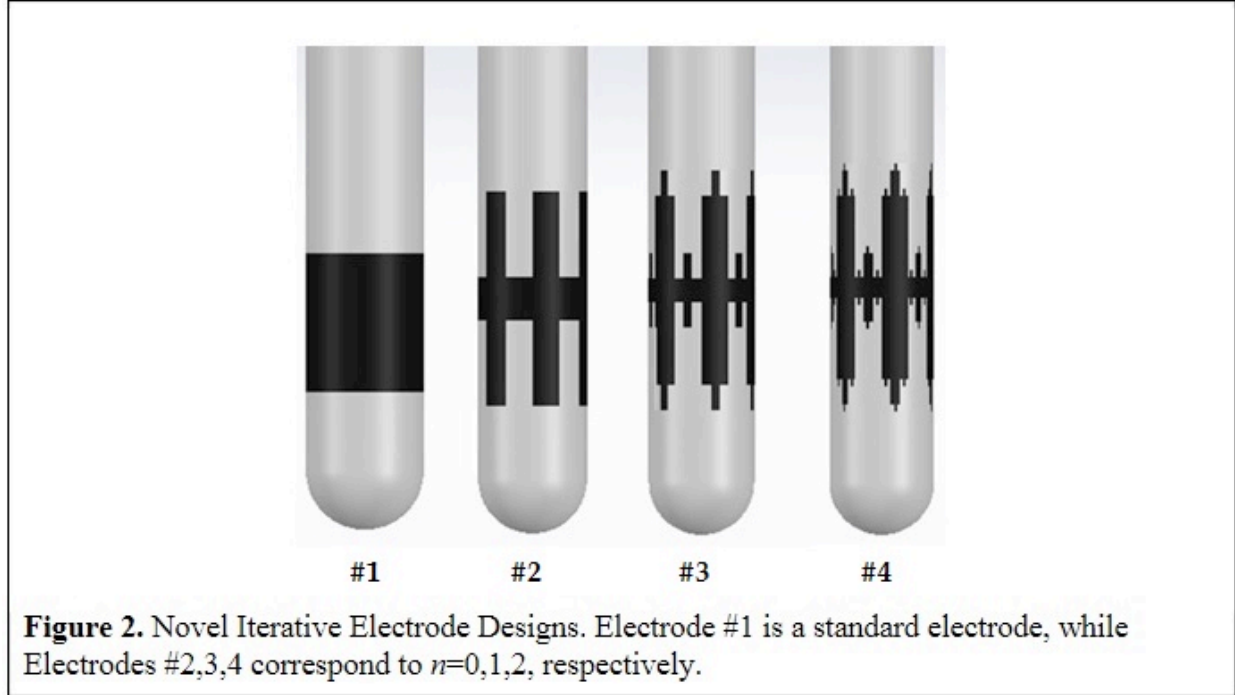
Using these formulas, electrode$_n$ can be constructed by:

1. Determining B_n and constructing the base around the contact circumference.
2. Adding protrusions of height P_0 mm and central angle $\theta_0=\pi/6$ and every $k\pi/6$ (k=odd or even integers) around the base circumference; this forms six repetitions in both vertical directions. (*Note*: arc length $s_{P0}=0.635\pi/6$ mm)
3. Sequentially adding protrusions of height $P_{1,2,...n}$ mm and central angles $\theta_{1,2,...n}=\pi/6(3^n)$ at the start (taken as a central angle distance of $\pi/6(3^n)$ from the end of any given P_0) of $\pi/2(3^n)$ intervals

around the resulting shape (i.e. to the middle of every horizontal edge resulting from all of the protrusion additions until that point, in both vertical directions). (*Note*: arc lengths $s_{P1,2,...n} = s_{P0}/(3^n)$ mm))

This method was used to create electrode contact geometries corresponding to iterations n=0,1,2

(Figure 2, Electrode #2,3,4, respectively).

Figure 2. Novel Iterative Electrode Designs. Electrode #1 is a standard electrode, while Electrodes #2,3,4 correspond to n=0,1,2, respectively.

The iterative method proved to dramatically increase perimeter with each fractal-like addition/subtraction-repetition (Chart 1).

FINITE ELEMENT MODEL OF ITERATIVE ELECTRODES

Each sequential electrode was imported into COMSOL Multiphysics 4.4 (COMSOL Inc, Burlington, MA), and placed into a homogeneous, isotropic, axisymmetric cylindrical model of height 100 mm, radius 50 mm, and a conductivity σ=0.2 S/m representative of a grey matter tissue medium (Yousif *et al.*, 2008; Faes *et al.*, 1999). Dirichlet boundary conditions were used to define the voltages of the active contact and the outer boundary of the tissue medium. The monopolar, cathodic electrode contact area potential was set to 1 V and a conductivity σ=10^7 S/m, while the insulators and outer tissue boundaries were set to a potential of 0 V, with the insulator conductivity σ=10^{-5} S/m.

Each electrode model was then partitioned into tetrahedral mesh elements, of element sizes of 10^{-5} m (for fine resolution of the relatively intricate contacts) to 10^{-2} m (for coarse resolution of the relatively uniform tissue medium). The potential distribution within the cylindrical tissue medium was determined by solving the Laplace equation, $\nabla^2 V_e$=0.

MULTICOMPARTMENT CABLE MODEL OF NEURONS

A three-dimensional array of 4,692 points with 0.3 mm spacing from -2.4 mm to 2.4 mm in the x, y, and z directions was constructed. Centers of 4,692 neurons consisting of sequential Nodes of Ranvier were placed tangent to the electrode circumference at these points. 100 Hz, 1 V IPG pulses of width 100 μs, in a 30 ms train consisting of 3 total pulses were simulated at the electrode contact in NEURON 7.3 (Volkmann *et al.*, 2002; NEURON, Yale University, New Haven, CT) i.e. the potential distribution derived in Comsol Multiphysics 3.5 in response to one, 1 V contact stimulus was extracted and interpolated for

this sequence. Responsive action potentials of myelinated axons with mammalian membrane dynamics were generated, and neuronal thresholds for the generation of action potentials were determined.

CALCULATION AND VISUALIZATION OF THE VOLUME OF TISSUE ACTIVATED
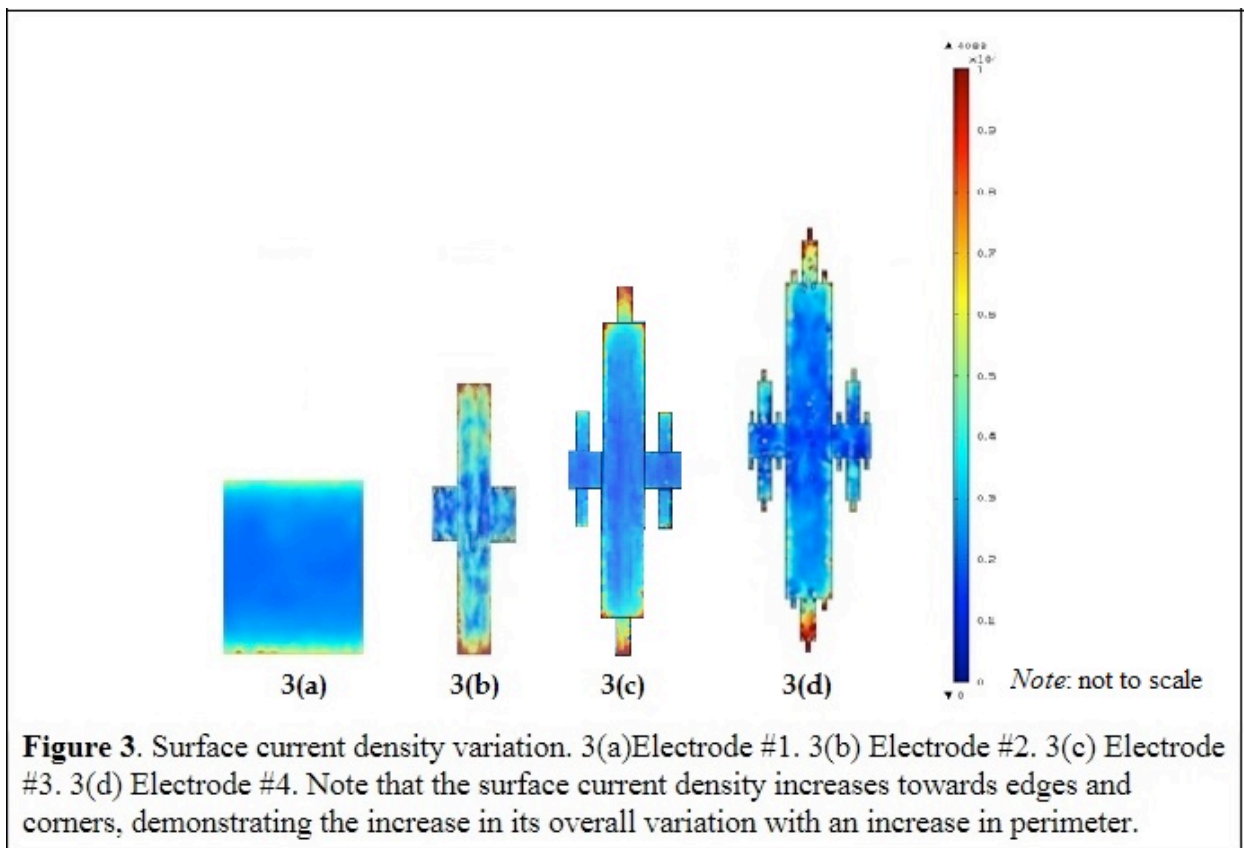
The activation thresholds of the neurons were interpolated in SCIRun 4.7 (SCIRun, University of Utah Center for Integrative Biomedical Computing, Salt Lake City, UT) to create a realistic activation profile with respect to distance from the electrode contact. This profile was used to create and calculate the volume of a three-dimensional solid with a spatial resolution of 0.1 mm^3 representing the VTA.

Visualization of VTA overlap with a human STN model (Allen Brain Atlas 3D Structures 2004, 2013 Allen Institute for Brain Science, Seattle, WA) was performed by placing the electrodes at a clinically-relevant 3-D angle, namely, a +60° anterior/posterior, +15° medial/lateral, and 0° superior/inferior angle with respect to the left, superior, anterior corner of the STN (Gross *et al.*, 2006). Implantation angles accounted for STN orientation offset.

RESULTS

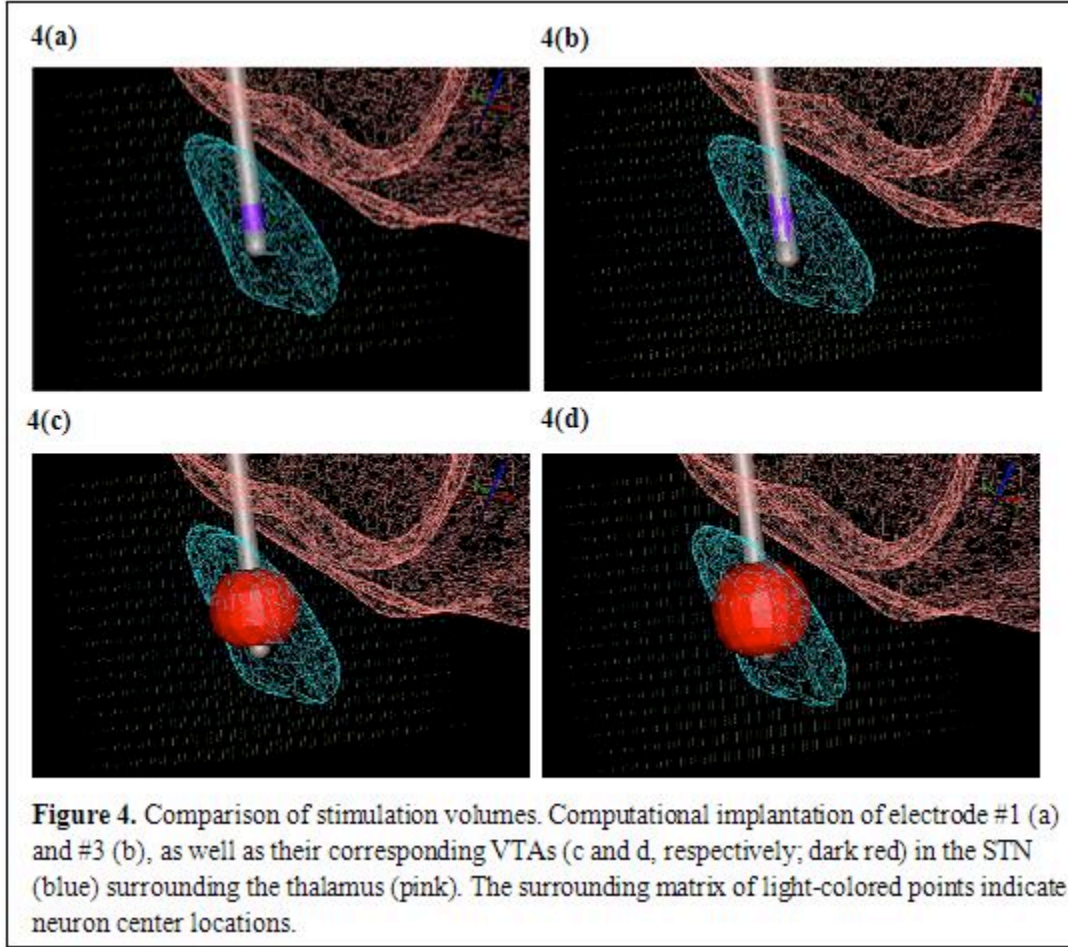### Current Density Distribution on Electrode Surfaces

The current density distributions on the surface of electrodes #1-#4 when a constant voltage of 1 V was applied are shown in Figure 3. The current density increased towards the perimeter of the electrodes. Each high-perimeter iterative electrode configuration yielded increased surface current density variation (Figure 3). The current density was uniform along the base's perimeters, while the current density was highly non-uniform along the protrusion perimeters, and was highest at the crests and lowest in the troughs of the protrusion perimeters.

Figure 3. Surface current density variation. 3(a)Electrode #1. 3(b) Electrode #2. 3(c) Electrode #3. 3(d) Electrode #4. Note that the surface current density increases towards edges and corners, demonstrating the increase in its overall variation with an increase in perimeter.

Stimulation Efficiency

At 1 V stimulation, electrode #2 (n=0) yielded a VTA of 85.551 mm^3, a 23.9% increase from that of a standard electrode (VTA: 69.013 mm^3); Electrode #3 (n=1) yielded a VTA of 88.564 mm^3, a 28.3% increase

from that of a standard electrode; Electrode #4 (n=2) yielded a VTA of 89.323 mm^3, a 29.4% increase from that of a standard electrode. These VTA's were then superimposed in the STN.

Figure 4. Comparison of stimulation volumes. Computational implantation of electrode #1 (a) and #3 (b), as well as their corresponding VTAs (c and d, respectively; dark red) in the STN (blue) surrounding the thalamus (pink). The surrounding matrix of light-colored points indicate neuron center locations.

DISCUSSION

We designed DBS electrodes whose contact geometries adhere to strictly defined iterative sequences to increase perimeter, surface current density variation, neuronal activating functions (measured by VTA), and subsequent power efficiency to increase the battery lifetime of DBS-IPGs. Our results indicate that this stepwise addition of small elements to a basic shape can increase VTA, as desired. Each design had a constant surface area with respect to a standard electrode, ensuring their meeting of safety regulations derived from potential tissue damage due to increased electrode charge density (Engler *et al.*, 2014).

Limitations of this study include that fact an encapsulation layer representing an envelope consisting of glial cells around the electrode, which increases the variety of surrounding tissue conductance, was neglected during finite element modeling (Kent *et al.*, 2014). Since the current study did not focus on the absolute stimulation efficiency of an electrode, but rather the comparative stimulation efficiency between electrodes with various geometries, we expect that including an encapsulation layer in the model would add the same effect on all of our electrode designs, and thus would not change the relative comparisons in terms of stimulation efficiency. Secondly, characteristic anisotropies and inhomogeneities of each DBS recipient were not taken into account (McIntyre *et al.*, 2004). Although the true biological volume conductor is inhomogeneous and anisotropic, one study of deep brain stimulation indicated that a homogenous isotropic model provided predictions of voltage distributions remarkably similar to a more detailed inhomogenous and anisotropic model for the expected region of stimulation around the electrode (Miocinovic *et al.*, 2009). Thirdly, the population of model neurons did not include

cell bodies, dendrites, or synaptic inputs. Although both experiment studies (Nowak *et al*, 1998 (1); Nowak *et al*, 1998 (2)) and computational models (McIntyre *et al*., 1999) indicate that during extracellular stimulation action potential initiation occurs in the axon, the impact of changes in geometry on the efficiency of activating other neural elements may differ from those of axons.

In summary, while the therapeutic mechanisms of DBS are not entirely understood, iterative reshaping of electrode contact surface area defined by mathematical sequences as a method of increasing contact perimeter holds promise for improving DBS stimulation efficiency.

ACKNOWLEDGEMENTS

REFERENCES
Benabid, A.L., Charbardes, S., Mitrofanis, J., and Pollak, P. (2009). Deep brain stimulation of the subthalamic nucleus for the treatment of Parkinson's disease. *Lancet Neurol.* 8(1), 67-81. doi: 10.1016/S1474-4422(08)70291-6.

Benabid, A.L., Koudsie, A., Benazzouz, A., Vercueil, L., Fraix, V., Chabardes, S., Lebas, J. F., and Pollak, P. (2001). Deep brain stimulation of the corpus luysi (subthalamic nucleus) and other targets in Parkinson's disease. Extension to new indications such as dystonia and epilepsy. *J. Neurol.* 248(Suppl 3), III37-III4.

Bhatia, S., Zhang, K., Oh, M., and Angle, C., Whiting, D. (2010). Infections and hardware salvage after deep brain stimulation surgery: a single-center study and review of the literature. *Stereotact. Funct. Neurosurg.* 88, 147–155. doi: 10.1159/000303528

Blahak, C., Capelle, H.H., Baezner, H., Kinfe, T.M., Hennerici, M.G., and Krauss, J.K. (2001). Battery lifetime in pallidal deep brain stimulation for dystonia. *Eur. J. Neurol.* 18(6), 872-5. doi: 10.1111/j.1468-1331.2010.03290.x.

Butson, C.R. and McIntyre, C.C. (2006). Role of electrode design on the volume of tissue activated during deep brain stimulation. *J. Neural Eng.* 3(1), 1-8.

Chopra, A., Klassen, B.T., and Stead, M. (2013). Current clinical application of deep-brain stimulation for essential tremor. *Neuropsychiatr. Dis. Treat.* 9, 1859-65. doi: 10.2147/NDT.S32342.

Coffrey, R.J. (2009). Deep brain stimulation devices: a brief technical history and review. *Artif. Organs.* 33(3), 208-20. doi: 10.1111/j.1525-1594.2008.00620.x.

Dorvad, A.D., Panjwani, N., Qi, R.Y., and Grill, W. M. (2009). Deep brain stimulation that abolishes Parkinsonian activity in basal ganglia improves thalamic relay fidelity in a computational circuit. *Conf. Proc. IEEE Eng. Med. Biol. Soc.* 2009, 4230-3. doi: 10.1109/IEMBS.2009.5333611.

Engler, G., Sharott, A., von Nicolai, C., Streichert, T., Papageorgiou, I., Schulte, A., Westphal, M., Lamszus, K., Engel, A.K., Moll, C.K.E., and Hamel, W. High-Frequency Stimulation of the Subthalamic Nucleus Counteracts Cortical Expression of Major Histocompatibility Complex Genes in a Rat Model of Parkinson's Disease. (2014). *P. O. Neural Eng.* 9(13), pages. doi:10.1371/journal.pone.0091663

Faes, T.J.C., van der Meij, H.A., Munck, J.C., and Heethaar, R.M. (1999). The electric resistivity of human tissues (100 Hz-10 MHz): a meta-analysis of review studies. *Physiol. Meas.* 20(4), R1-10.

Fontaine, D., Mattei, V., Borg, M., von Langsdorff, D., Magnie, M.N., Chanalet, S., Robert, P., and Paquis, P. (2004). Effect of subthalamic nucleus stimulation on   obsessive-compulsive disorder in a patient with Parkinson disease. Case report. *J. Neurosurg.* 100(6), 1084-6.

Golestanirad, L., Elahi, B., Molina, A., Mosig, J.R., Pollo, C., Chen, R., and Graham, S.J. (2013). Analysis of fractal electrodes for efficient neural stimulation. *Front. Neuroeng.* 6, 3. doi: 10.3389/fneng.2013.00003.

Groiss, S.J., Wojtecki, L., Sudmeyer, M., and Schnitzler, A. (2009). Deep brain stimulation in Parkinson's disease. *Ther. Adv. Neurol. Disord.* 2, 20–28. doi: 10.1177/1756285609339382

Gross, R.E., Krack, P., Rodriguez-Oroz, M.C., Rezai, A.R., and Benabid, A.L. (2006). Electrophysiological mapping for the implantation of deep brain stimulators for Parkinson's disease and tremor. *Mov. Disord.* 21(S14), S259-S283.

Holtzheimer III, P.E., Mayberg, H.S. (2010). Deep Brain Stimulation for Treatment-Resistant Depression. *Am. J. Psychiatry.* 167, 1437-1444. doi:10.1176/appi.ajp.2010.10010141

Hu, W. and Stead, M. (2014). Deep brain stimulation for dystonia. *Transl. Neurodegener.* 3, 2. doi: 10.1186/2047-9158-3-2

Kawakami, N., Jessen, J., Bordini, B., Gallagher, C., Klootwyk, J., Garell, C.P. (2005). Deep brain stimulation of the subthalamic nucleus in Parkinson's disease. *W.M.J.* 104(6), 35-8.

Kent, A.R., Swan, B.D., Brocker, D.T., Turner, D.A., Gross, R.E., and Grill, W.M. (2014).   Measurement of evoked potentials during thalamic deep brain stimulation. *Brain Stim. J.* doi: http://dx.doi.org/10.1016/j.brs.2014.09.017

McIntyre, C.C. and W.M. Grill, Excitation of central nervous system neurons by nonuniform electric fields. *Biophys. J.,* 1999. 76(2): p. 878-88.

McIntyre, C.C., Mori, S., Sherman, D.L., Thakor, N.V., Vitek, J.L. (2004). Electric field and stimulating influence generated by deep brain stimulation of the subthalamic nucleus. *Clin. Neurophysiol.* 115(3), 589-95.

Miocinovic, S., et al., Experimental and theoretical characterization of the voltage distribution generated by deep brain stimulation. *Exp. Neurol.,* 2009. 216(1): p. 166-76.

Nowak, L.G. and J. Bullier, Axons, but not cell bodies, are activated by electrical stimulation in cortical gray matter. Ii. Evidence from selective inactivation of cell bodies and axon initial segments. *Exp. Brain. Res.,* 1998. 118(4): p. 489-500.

Nowak, L.G. and J. Bullier, Axons, but not cell bodies, are activated by electrical stimulation in cortical gray matter. I. Evidence from chronaxie measurements. *Exp. Brain. Res.,* 1998. 118(4): p. 477-88.

Rattay. F. (1989). Analysis of models for extracellular fiber stimulation. *IEEE Trans. Biomed. Eng.* 36(7),676-82.

Russman, H., Ghika, J., Combrement, P., Villemure, J.G., Bogousslavsky, J., Burkhard, P.R., Vingerhoets, F.J.G. (2004). l-Dopa-induced dyskinesia improvement after STN-DBS depends upon medication reduction. *Neurology.* 63(1), 153-5. doi: 10.1212/01.WNL.0000131910.72829.9D.

Volkmann, J., Herzog, J., Kopper, F., and Deuschl, G. (2002). Introduction to the   programming of deep brain stimulators. *Mov. Disord.* 17(Suppl 3), S181-7.

Yousif, N., Bayford, R., and Liu, X. (2008). The influence of reactivity of the electrode-brain interface on the crossing electric current in therapeutic deep brain stimulation. *Neuroscience.* 156(3), 597-606.

Wei, X.F. and Grill, W.M. (2009). Analysis of high-perimeter planar electrodes for efficient neural stimulation. *Front. Neuroeng.* 2, 15. doi: 10.3389/neuro.16.015.2009.